Spin-Crossover in $[Fe(3\text{-bpp})_2][BF_4]_2$ in Different Solvents – a Dramatic Stabilisation of the Low-Spin State in Water

Simon A. Barrett, Colin A. Kilner and Malcolm A. Halcrow*

School of Chemistry, University of Leeds, Woodhouse Lane, Leeds, UK LS2 9JT.
E-mail: m.a.halcrow@leeds.ac.uk

Electronic Supplementary Information

Experimental details

Table S1 Experimental details for the single crystal structure determinations of solvates of $[Fe(3\text{-bpp})_2][BF_4]_2$.

Table S2 Selected bond lengths and angles in the crystal structures of $[Fe(3\text{-bpp})_2][BF_4]_2{\cdot}3(C_2H_5)_2O$ and $[Fe(3\text{-bpp})_2][BF_4]_2{\cdot}2CH_3NO_2{\cdot}2(C_3H_7)_2O$.

Figure S1 Views of the hydrogen-bonded moieties in $[Fe(3\text{-bpp})_2][BF_4]_2{\cdot}3(C_2H_5)_2O$ and $[Fe(3\text{-bpp})_2][BF_4]_2{\cdot}2CH_3NO_2{\cdot}2(C_3H_7)_2O$, showing the atom numbering schemes employed.

Table S3 Selected bond lengths and angles in the crystal structures of $[Fe(3\text{-bpp})_2][BF_4]_2{\cdot}2CH_3NO_2$ and $[Fe(3\text{-bpp})_2][BF_4]_2{\cdot}2CH_3CN$.

Figure S2 Views of the formula units in the crystal structures of $[Fe(3\text{-bpp})_2][BF_4]_2{\cdot}2CH_3NO_2$ and $[Fe(3\text{-bpp})_2][BF_4]_2{\cdot}2CH_3CN$, showing the atom numbering schemes employed.

Table S4 Hydrogen bond parameters in the crystal structure in this work.

Table S5 ^{1}H NMR data for $[Fe(3\text{-bpp})_2][BF_4]_2$ in different solvents.

Table S6 ^{1}H NMR data for $[Fe(1\text{-bpp})_2][BF_4]_2$ in different solvents.

Figure S3 Plots of the ^{1}H NMR data of $[Fe(3\text{-bpp})_2][BF_4]_2$ against different solvent polarity or basicity scales.

Figure S4 Comparison of the solvent dependence of the ^{1}H isotropic shifts of $[Fe(3\text{-bpp})_2][BF_4]_2$ and $[Fe(1\text{-bpp})_2][BF_4]_2$.

Figure S5 Comparison of spin-crossover of $[Fe(3\text{-bpp})_2][BF_4]_2$ and $[Fe(1\text{-bpp})_2][BF_4]_2$ by Evans method.

Table S7 UV/vis data of $[Fe(3\text{-bpp})_2][BF_4]_2$ in different solvents

Figure S6 Variation of the spin-state population at room temperature for $[Fe(3\text{-bpp})_2][BF_4]_2$ with solvent composition in the water/acetone solvent mixtures.

Figure S7 Correlation between the Evans method and UV/vis data for $[Fe(3\text{-bpp})_2][BF_4]_2$ in the water/acetone solvent mixtures.

References.

Experimental

$[Fe(3\text{-bpp})_2][BF_4]_2$[1] and $[Fe(1\text{-bpp})_2][BF_4]_2$[2] were synthesised by the published methods. All other reagents and solvents were used as commercially supplied, without further purification.

Single crystal *X*-ray structure determinations

Brown single crystals of $[Fe(3\text{-bpp})_2][BF_4]_2\cdot 3(C_2H_5)_2O$ were grown by slow diffusion of diethyl ether vapour into a nitromethane solutions of the complex. A similar vapour diffusion using di-*iso*propyl ether as antisolvent yielded a mixture of $[Fe(3\text{-bpp})_2][BF_4]_2\cdot 2CH_3NO_2\cdot 2(C_3H_7)_2O$ and $[Fe(3\text{-bpp})_2][BF_4]_2\cdot 2CH_3NO_2$, while crystallisation from acetonitrile/di-*iso*propyl ether afforded $[Fe(3\text{-bpp})_2][BF_4]_2\cdot 2CH_3CN$ only. Experimental details of these structure determinations are given in Table S1. All diffraction data were measured using a Bruker X8 Apex diffractometer, with graphite-monochromated Mo-K_α radiation (λ = 0.71073 Å) generated by a rotating anode. The diffractometer was fitted with an Oxford Cryostream nitrogen low temperature device. The structures were solved by a Patterson synthesis ($[Fe(3\text{-bpp})_2][BF_4]_2\cdot 3(C_2H_5)_2O$) or by direct methods (the other structures) using SHELXS97,[3] and developed by full least-squares refinement on F^2 (*SHELXL97*[3]). Crystallographic figures were prepared using *XSEED*,[4] which incorporates *POVRAY*.[5]

The unit cell of $[Fe(3\text{-bpp})_2][BF_4]_2\cdot 3(C_2H_5)_2O$ contains one formula unit, with each moiety lying on a general crystallographic position. No disorder was detected during refinement of either structure, and no restraints were applied. All non-H atoms were refined anisotropically, while H atoms were placed in calculated positions and refined using a riding model.

The crystals $[Fe(3\text{-bpp})_2][BF_4]_2\cdot 2CH_3NO_2$ and $[Fe(3\text{-bpp})_2][BF_4]_2\cdot 2CH_3CN$ are isomorphous, containing half a complex dication with Fe(1), N(2), C(5), N(11) and C(14) all lying on the crystallographic C_2 axis [½, *y*, ¾]; and, one BF_4^- anion and one solvent molecule, both occupying general lattice sites. The anion in the nitromethane solvate is disordered over three equally occupied orientations, while in the acetonitrile solvate the anion is disordered over two sites whose occupancy ratio refined to 0.67:0.33. In both structures the refined restraints B–F = 1.40(2) and F...F = 2.29(2) Å were applied to the partial anions. The solvent molecule in the acetonitrile molecule is also disordered, over two equally occupied sites. These were refined with the fixed restraints C–C = 1.46(2), C≡N = 1.16(2) and 1,3-C...N = 2.62(2) Å. The solvent molecule in the nitromethane solvate is crystallographically ordered. All non-H atoms with occupancy ≥0.5 were refined anisotropically in these structures, and H atoms were placed in calculated positions and refined using a riding model.

The unit cell of $[Fe(3\text{-bpp})_2][BF_4]_2\cdot 2CH_3NO_2\cdot 2(C_3H_7)_2O$ contains one formula unit, with each moiety lying on a general crystallographic position. One of the two BF_4^- ions is disordered over three sites with occupancies of 0.40, 0.40 and 0.20. The refined restraints B–F = 1.37(2) and F...F = 2.24(2) Å were applied to this anion. The other anion was refined as ordered, although a high displacement parameter on one F atom may indicate some unresolved disorder in that moiety as well. One nitromethane molecule is also disordered, over two orientations with a 0.60:0.40 occupancy ratio. These two partial solvent sites share a common wholly occupied O atom O(65) (which accepts a hydrogen bond from the complex cation). This was modelled using the fixed restraints C–N = 1.47(2), N–O = 1.21(2), O...O = 2.10(2) and C...O = 2.30(2) Å. All wholly occupied non-H atoms were refined anistropically, and all H atoms were placed in calculated positions and refined using a riding model.

Other measurements

UV/visible spectra were obtained with a Perkin-ElmerLambda 900 spectrophotometer operating between 200–1,500 nm, in 1 cm quartz cells. Magnetic susceptibility measurements in solution were obtained by Evans method using a Bruker DRX500 spectrometer operating at 500.13 MHz.[6] *Tert*butanol was used as the internal standard for the measurements in D_2O, while tetramethylsilane was the internal standard in other solvents. A diamagnetic correction for the sample,[7] and a correction for the variation of the density of the solvent with temperature,[8] were applied to these data. All magnetochemical data manipulation and graph plotting was carried out using *SIGMAPLOT*.[9]

Table S1 Experimental details for the single crystal structure determinations of solvates of $[Fe(3\text{-bpp})_2][BF_4]_2$.

	$[Fe(3\text{-bpp})_2][BF_4]_2\cdot 3(C_2H_5)_2O$	$[Fe(3\text{-bpp})_2][BF_4]_2\cdot 2CH_3NO_2$	$[Fe(3\text{-bpp})_2][BF_4]_2\cdot 2CH_3NO_2\cdot 2(C_3H_7)_2O$	$[Fe(3\text{-bpp})_2][BF_4]_2\cdot 2CH_3CN$
Molecular formula	$C_{34}H_{48}B_2F_8FeN_{10}O_3$	$C_{24}H_{24}B_2F_8FeN_{12}O_4$	$C_{36}H_{52}B_2F_8FeN_{12}O_6$	$C_{26}H_{24}B_2F_8FeN_{12}$
M_r	874.29	774.02	978.37	734.04
Crystal class	Monoclinic	Monoclinic	Monoclinic	Monoclinic
Space group	*C*2/*c*	*C*2/*c*	$P2_1/n$	*C*2/*c*
a (Å)	23.953(5)	11.721(2)	13.035(3)	11.8232(13)
b (Å)	9.962(2)	22.987(5)	13.729(3)	23.510(2)
c (Å)	36.531(7)	12.442(3)	26.943(5)	12.3117(14)
β (°)	103.25(3)	93.26(3)	102.22(3)	93.191(6)
V (Å^3)	8485(3)	3346.7(12)	4712.4(16)	3416.9(6)
Z	8	4	4	4
μ (Mo-K□) (mm^{-1})	0.436	0.546	0.407	0.523
T (K)	150(2)	150(2)	150(2)	150(2)
Measured reflections	6 922	29057	76956	30470
Independent reflections	968	4108	12045	4318
R_{int}	0.059	0.051	0.048	0.056
$R(F)$,[a] $I > 2\sigma(I)$	0.058	0.040	0.057	0.053
w$R(F^2)$,[b] all data	0.164	0.111	0.159	0.158
Goodness of fit	1.053	1.045	1.036	1.033

[a] $R = \Sigma[\,|F_o| - |F_c|\,] / \Sigma|F_o|$ [b] $wR = [\Sigma w(F_o^2 - F_c^2) \;/\; \Sigma wF_o^4]^{½}$

Table S2 Selected bond lengths and angles in the crystal structures of $[Fe(3\text{-bpp})_2][BF_4]_2\cdot 3(C_2H_5)_2O$ and $[Fe(3\text{-bpp})_2][BF_4]_2\cdot 2CH_3NO_2\cdot 2(C_3H_7)_2O$ (Å, °). See Fig. S1 for the atom numbering Scheme employed.

	$[Fe(3\text{-bpp})_2][BF_4]_2\cdot 3(C_2H_5)_2O$	$[Fe(3\text{-bpp})_2][BF_4]_2\cdot 2CH_3NO_2\cdot 2(C_3H_7)_2O$
Fe(1)–N(2)	2.068(2)	1.9394(19)
Fe(1)–N(9)	2.127(2)	1.988(2)
Fe(1)–N(14)	2.137(3)	1.980(2)
Fe(1)–N(18)	2.069(2)	1.939(2)
Fe(1)–N(25)	2.109(2)	1.964(2)
Fe(1)–N(30)	2.113(3)	1.996(2)
N(2)–Fe(1)–N(9)	75.54(9)	79.18(8)
N(2)–Fe(1)–N(14)	75.56(10)	79.04(8)
N(2)–Fe(1)–N(18)	174.36(9)	177.46(8)
N(2)–Fe(1)–N(25)	104.03(9)	98.42(8)
N(2)–Fe(1)–N(30)	105.54(9)	103.33(8)
N(9)–Fe(1)–N(14)	151.09(9)	158.22(8)
N(9)–Fe(1)–N(18)	98.89(9)	101.56(8)
N(9)–Fe(1)–N(25)	94.38(9)	90.69(8)
N(9)–Fe(1)–N(30)	94.04(9)	93.05(8)
N(14)–Fe(1)–N(18)	109.99(9)	100.20(8)
N(14)–Fe(1)–N(25)	91.69(9)	92.69(9)
N(14)–Fe(1)–N(30)	94.49(9)	91.74(8)
N(18)–Fe(1)–N(25)	75.30(9)	79.17(9)
N(18)–Fe(1)–N(30)	75.39(9)	79.08(8)
N(25)–Fe(1)–N(30)	150.41(9)	158.24(8)

These data imply that $[Fe(3\text{-bpp})_2][BF_4]_2\cdot 2CH_3NO_2\cdot 2(C_3H_7)_2O$ is low spin at the temperature of measurement (150 K), but that $[Fe(3\text{-bpp})_2][BF_4]_2\cdot 3(C_2H_5)_2O$ has a mixed high:low-spin state population.

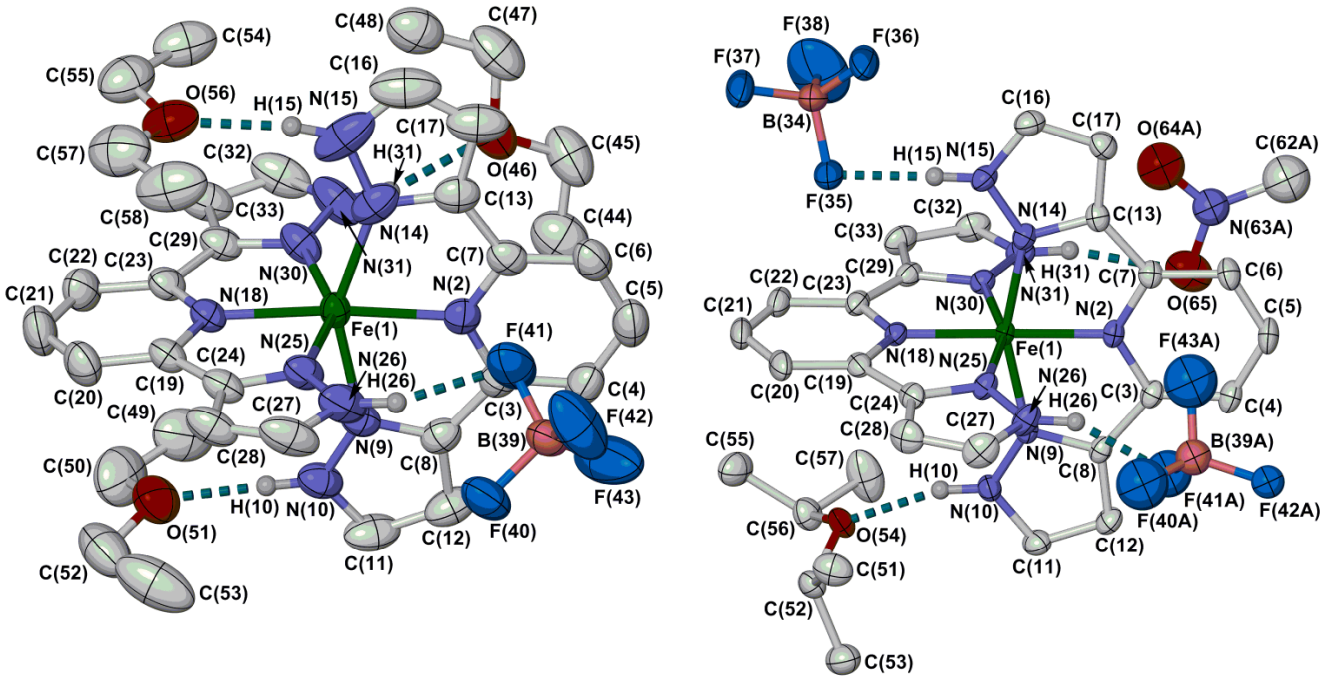

Fig. S1 Views of the hydrogen-bonded moieties in $[Fe(3\text{-bpp})_2][BF_4]_2\cdot 3(C_2H_5)_2O$ (left) and $[Fe(3\text{-bpp})_2][BF_4]_2\cdot 2CH_3NO_2\cdot 2(C_3H_7)_2O$ (right), showing the atom numbering schemes employed. Thermal ellipsoids are at the 50% probability level, and all C-bound H atoms are omitted. Residues that are not involved in hydrogen-bonding interactions are not shown, and only one orientation of the disordered residues is included.

Colour code: C, white; H, grey; B, pink; F, cyan; Fe, green; N, blue; O, red.

Table S3 Selected bond lengths and angles in the crystal structures of $[Fe(3\text{-bpp})_2][BF_4]_2\cdot 2CH_3NO_2$ and $[Fe(3\text{-bpp})_2][BF_4]_2\cdot 2CH_3CN$ (Å, °). See Fig. S2 for the atom numbering scheme employed. Symmetry code (i) $1–x, y, {}^3/_2–z$.

	$[Fe(3\text{-bpp})_2][BF_4]_2\cdot 2CH_3NO_2$	$[Fe(3\text{-bpp})_2][BF_4]_2\cdot 2CH_3CN$
Fe(1)–N(2)	1.962(2)	2.095(3)
Fe(1)–N(7)	1.9977(15)	2.144(2)
Fe(1)–N(11)	1.967(2)	2.106(3)
Fe(1)–N(16)	2.0111(15)	2.143(2)
N(2)–Fe(1)–N(7)	78.97(5)	75.70(7)
N(2)–Fe(1)–N(11)	180	180
N(2)–Fe(1)–N(16)	101.13(4)	104.72(6)
N(7)–Fe(1)–N(7^i)	157.94(9)	151.40(15)
N(7)–Fe(1)–N(11)	101.03(5)	104.30(7)
N(7)–Fe(1)–N(16)	90.67(6)	92.50(8)
N(7)–Fe(1)–N(16^i)	93.57(6)	94.69(8)
N(11)–Fe(1)–N(16)	78.87(4)	75.28(6)
N(16)–Fe(1)–N(16^i)	157.73(9)	150.56(12)

From these data, $[Fe(3\text{-bpp})_2][BF_4]_2\cdot 2CH_3NO_2$ is low spin at the temperature of measurement (150 K), but $[Fe(3\text{-bpp})_2][BF_4]_2\cdot 2CH_3CN$ has a mixed high:low-spin state population.

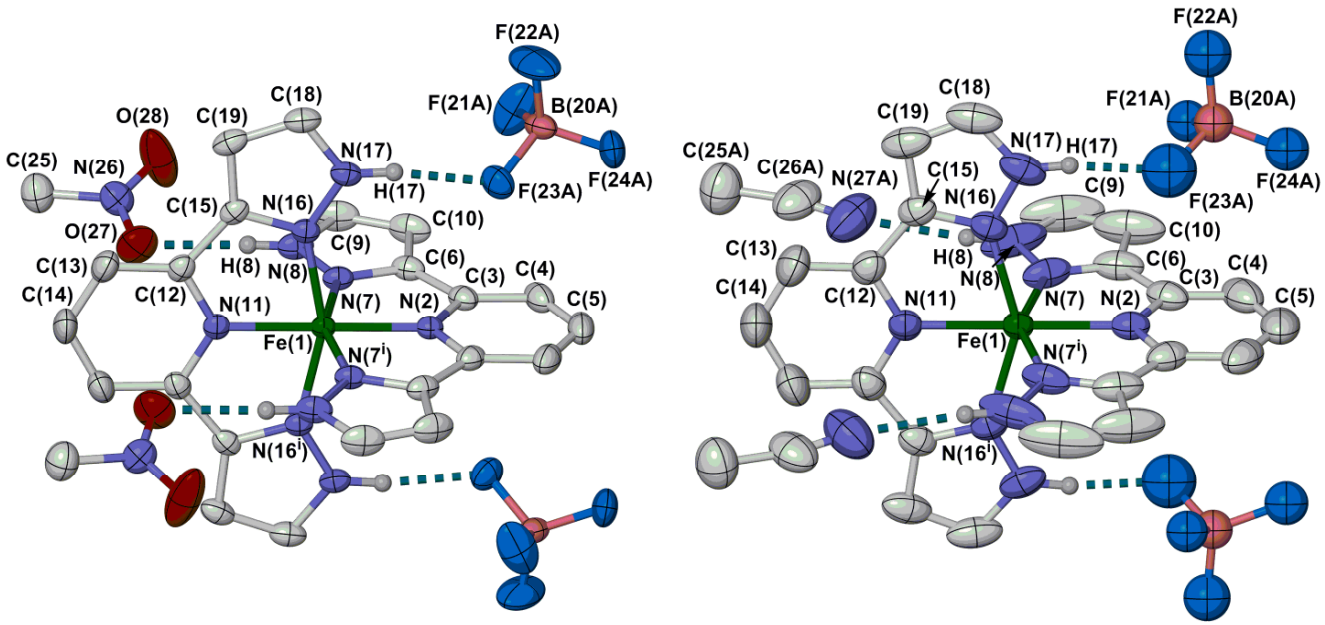

Fig. S2 Views of the formula units in the crystal structures of $[Fe(3\text{-bpp})_2][BF_4]_2\cdot 2CH_3NO_2$ (left) and $[Fe(3\text{-bpp})_2][BF_4]_2\cdot 2CH_3CN$ (right), showing the atom numbering schemes employed. Thermal ellipsoids are at the 50% probability level, all C-bound H atoms are omitted, and only the major orientations of the disordered residues are shown. Symmetry code: (i) $1–x, y, {}^3/_2–z$.

Colour code: C, white; H, grey; B, pink; F, cyan; Fe, green; N, blue; O, red.

Table S4 Hydrogen bond parameters in the crystal structures in this work (Å, º). See Figs. S1 and S2 for the atom numbering schemes employed.

	N–H	H...X	N…X	N–H…X
$[Fe(3\text{-}bpp)_2][BF_4]_2\cdot 3(C_2H_5)_2O$				
N(10)–H(10)…O(51)	0.88	1.84	2.715(4)	169.8
N(15)–H(15)…O(56)	0.88	1.97	2.836(5)	167.0
N(26)–H(26)…F(41)	0.88	1.99	2.843(3)	163.5
N(31)–H(31)…O(46)	0.88	1.99	2.808(4)	155.1
$[Fe(3\text{-}bpp)_2][BF_4]_2\cdot 2CH_3NO_2$				
N(8)–H(8)…O(27)	0.88	2.05	2.932(3)	175.2
N(17)–H(17)…F(23A)/F23(B)	0.88	1.93/1.85	2.800(6)/2.702(12)	170.2/163.6
$[Fe(3\text{-}bpp)_2][BF_4]_2\cdot 2CH_3NO_2\cdot 2(C_3H_7)_2O$				
N(10)–H(10)…O(54)	0.88	1.90	2.752(3)	163.0
N(15)–H(15)…F(35)	0.88	1.89	2.769(3)	175.0
N(26)–H(26)…F(41A)/F(41B)/F(41C)	0.88	1.89/1.97/2.12	2.704(7)/2.849(5)/2.948(8)	152.8/172.3/156.1
N(31)–H(31)…O(65)	0.88	2.18	3.037(4)	163.9
N(31)–H(31)…O(64A)[a]	0.88	2.41	3.073(6)	132.8
$[Fe(3\text{-}bpp)_2][BF_4]_2\cdot 2CH_3CN$				
N(8)–H(8)…N(27A)/N(27B)	0.88	2.20/1.84	3.072(15)/2.700(15)	172.9/163.9
N(17)–H(17)…F(23A)/F23(B)/F23(C)	0.88	1.86/1.88/1.99	2.734(13)/2.711(11)/2.838(9)	171.4/155.7/161.4

[a]In the other disorder site for this solvent molecule, O(64B) lies outside the hydrogen bonding distance from this N–H group.

Table S5 ^{1}H NMR data for $[Fe(3\text{-bpp})_2][BF_4]_2$ (**1[BF$_4$]$_2$**) in different solvents. These data are plotted in Figs. S3 and S4.

	E_N^T [10]	*DN* [11,12]	*SB* [13]	β [12,14]	Py H^4	N*H*	Py $H^{3/5}$	Pz H^4 & Pz H^5
D_2O	1.000	19.5	*n/a*	0.18	13.3	–	26.6	30.2, 30.2
CD_3OD	0.762	19.1	0.545	0.62	18.2	–	42.4	49.6, 50.1
C_2D_5OD	0.654	32.0	0.658	0.77	18.4	–	43.2	50.7, 51.4
CD_3NO_2	0.481	2.7	0.236	0.06	17.8	34.5	46.2	53.6, 55.2
CD_3CN	0.460	14.1	0.286	0.31	18.3	33.0	45.3	52.8, 53.8
$(CD_3)_2SO$[a]	0.444	29.8	0.647	0.76	17.7	31.0	39.9	46.7, 48.3
$DC(O)N(CD_3)_2$	0.386	26.6	0.613	0.69	18.6	32.4	41.9	49.0, 49.6
$(CD_3)_2CO$	0.355	17.0	0.475	0.48	18.0	33.3	43.4	50.5, 51.5

[a]Spectrum also contains a second minor paramagnetic 3-bpp-containing species (*ca.* 6 % by integral), and broad peaks assignable to free 3-bpp at 6.9, 7.6, 7.7 and 7.8 ppm with a 2:2:2:1 integral ratio. This is evidence for partial dissociation of the complex in this solvent.

Table S6 ^{1}H NMR data for $[Fe(1\text{-bpp})_2][BF_4]_2$ (**2[BF$_4$]$_2$**) in different solvents. These data are plotted in Fig. S4.

	E_N^T [10]	*DN* [11,12]	*SB* [13]	β [12,14]	Py H^4	Pz H^3 & Py $H^{3/5}$	Pz H^4 & Pz H^5
D_2O[a]	1.000	19.5	*n/a*	0.18	–	–	–
CD_3OD[b]	0.762	19.1	0.545	0.62	–3.5	48.7, 59.1	65.1, 69.1
C_2D_5OD[c]	0.654	32.0	0.658	0.77	–	–	–
CD_3NO_2	0.481	2.7	0.236	0.06	2.8	34.3, 36.3	56.7, 61.3
CD_3CN	0.460	14.1	0.286	0.31	2.6	34.6, 36.6	56.9, 61.7
$(CD_3)_2SO$[a]	0.444	29.8	0.647	0.76	–	–	–
$DC(O)N(CD_3)_2$[a]	0.386	26.6	0.613	0.69	–	–	–
$(CD_3)_2CO$	0.355	17.0	0.475	0.48	2.7	36.2, 37.9	57.8, 62.6

[a]Complex spontaneously decomposes to free ligand upon contact with this solvent. [b]Spectrum also contains broad peaks at 6.1 and 7.8 ppm in a 1:3 integral ratio, assignable to free 1-bpp. This is evidence for partial dissociation of the complex in this solvent. [c]Complex is insufficiently soluble in this solvent.

Reichardt's E_N^T parameter is a widely-used indicator of solvent polarity.[10] The Gutmann donor number (DN) is a measure of the Lewis basicity of a solvent;[11,12] Catalan's SB parameter describes its Brønsted basicity;[13] and, Kamlet and Taft's β parameter is a common measure of the hydrogen-bond acceptor character of the solvent.[14]

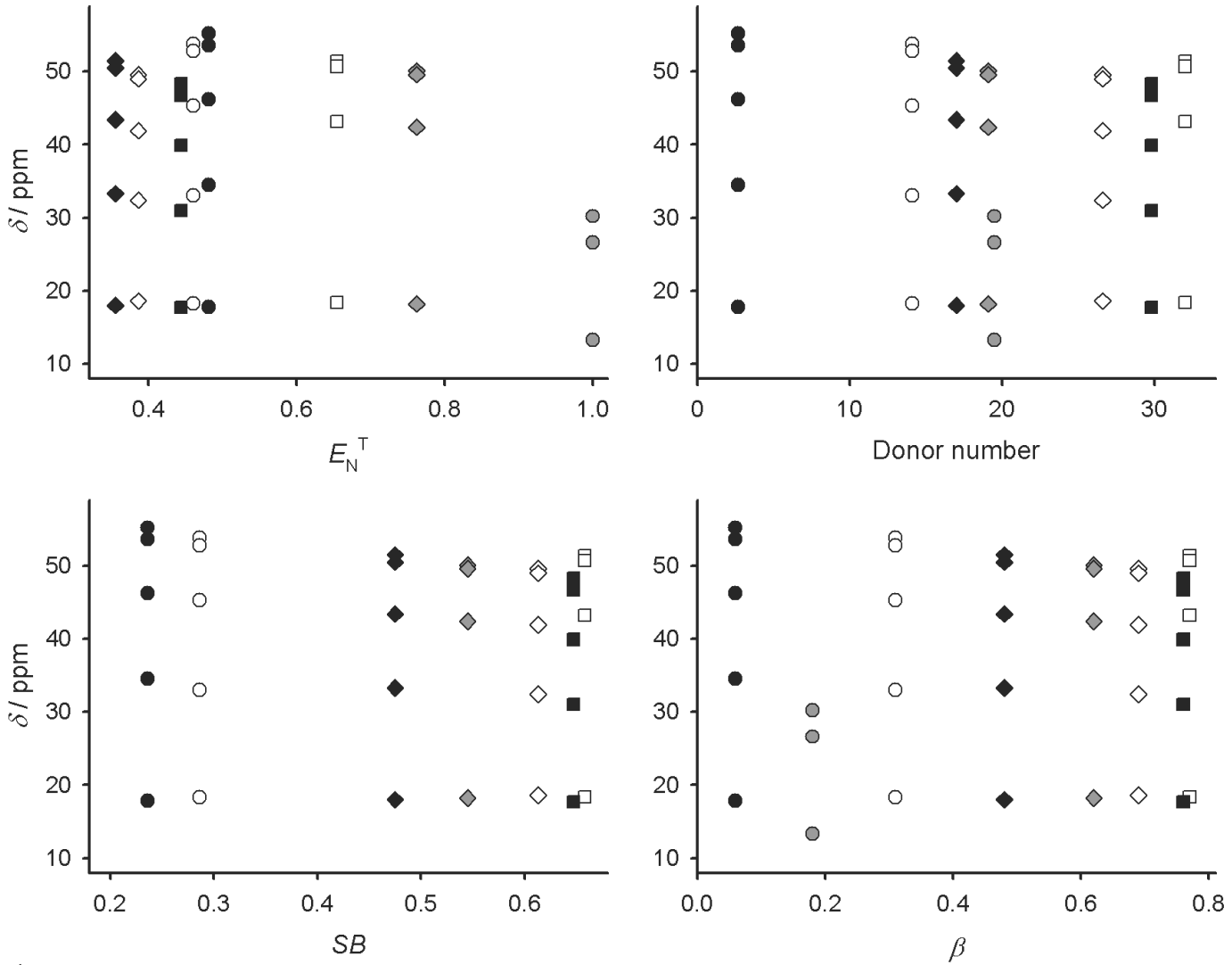

Fig. S3 Plots of the ^{1}H isotropic shifts of $[Fe(3\text{-bpp})_2][BF_4]_2$ (**1[BF$_4$]$_2$**) against different solvent polarity or basicity scales, in in CD_3NO_2 (●), D_2O (●), CD_3CN (○), $(CD_3)_2CO$ (◆), CD_3OD (◆), $(CD_3)_2NCDO$ (◇), $(CD_3)_2SO$ (■) and C_2D_5OD (□) (Table S5).

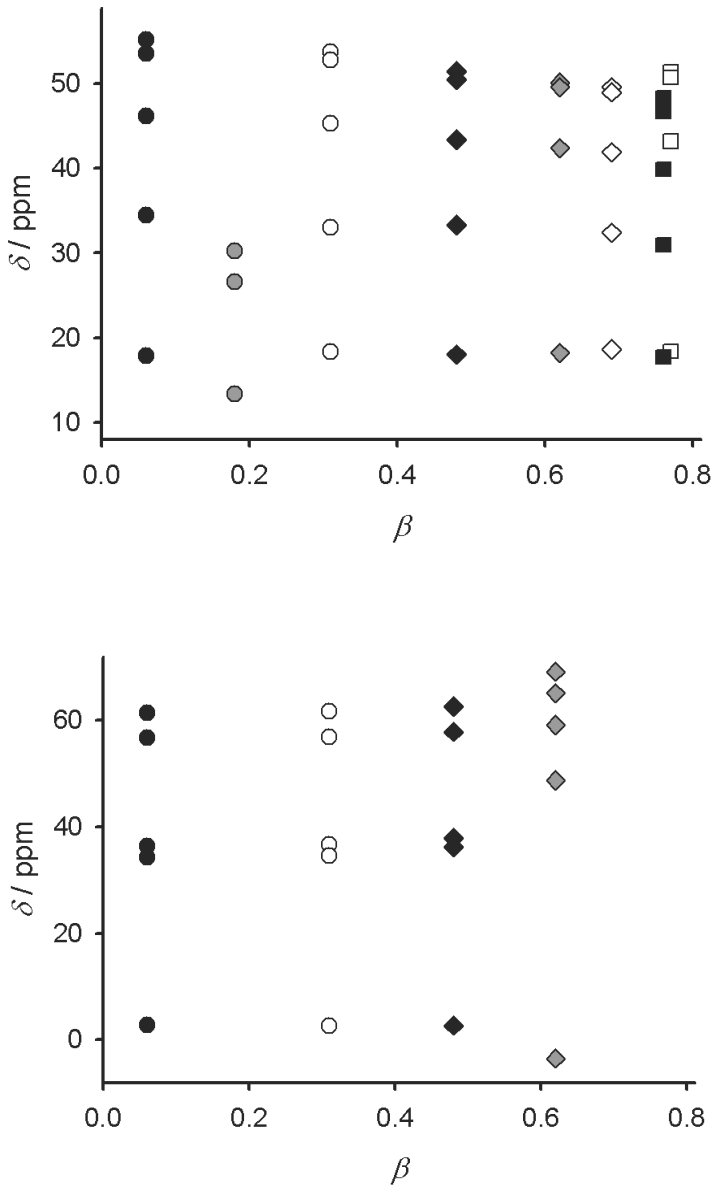

Fig. S4 Comparison of the solvent dependence of the ^{1}H isotropic shifts of $[Fe(3\text{-bpp})_2][BF_4]_2$ (**1[BF$_4$]$_2$**; top) and $[Fe(1\text{-bpp})_2][BF_4]_2$ (**2[BF$_4$]$_2$**; bottom) in CD_3NO_2 (●), D_2O (●), CD_3CN (○), $(CD_3)_2CO$ (◆), CD_3OD (◆), $(CD_3)_2NCDO$ (◇), $(CD_3)_2SO$ (■) and C_2D_5OD (□) (Tables S5 and S6). The graph for **1[BF$_4$]$_2$** is the same as in Fig. S3.

The increased isotropic shifts for **2[BF$_4$]$_2$** in CD_3OD are a consequence of partial decomposition of the complex in that solvent (the spectrum also contains a significant amount of free 1-bpp ligand).

Otherwise, there is no solvent dependence in the spectrum of **2[BF$_4$]$_2$** comparable to that exhibited by **1[BF$_4$]$_2$**.

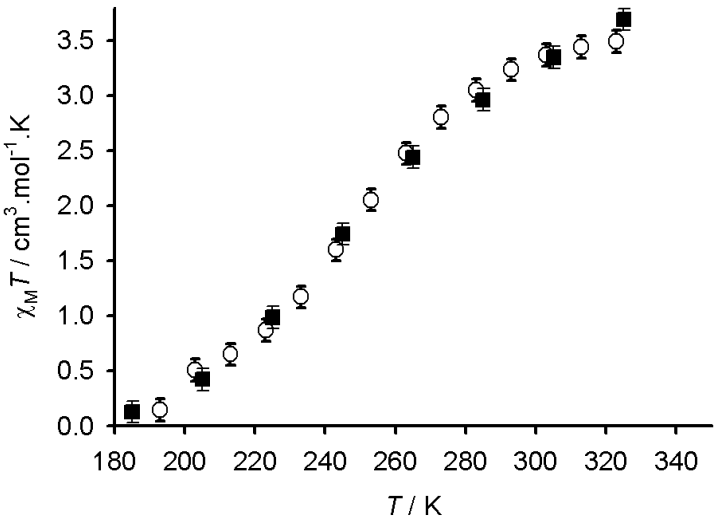

Fig. S5 Comparison of spin-crossover of $[Fe(3\text{-bpp})_2][BF_4]_2$ (**1[BF$_4$]$_2$**, ○) and $[Fe(1\text{-bpp})_2][BF_4]_2$ (**2[BF$_4$]$_2$**, ■) in $(CD_3)_2CO$. Data for **2[BF$_4$]$_2$** are taken from ref. 2.

The two curves are identical within experimental error, showing that the hydrogen-bonding capability of $[Fe(3\text{-bpp})_2][BF_4]_2$ has no impact on spin-crossover in this solvent.

Table S7 UV/vis data for the MLCT envelope of $[Fe(3\text{-bpp})_2][BF_4]_2$ in different solvents (Fig. S7, and Fig. 2 in the main paper). In addition to these peak maxima, shoulder absorptions around 530, 425 and (where not listed as a defined peak) 395 nm are present in all the spectra.

	Low-spin fraction of the sample at 293 K by Evans method	λ_{max}, nm (ε_{max}, 10^3 dm^3 mol^{-1} cm^{-1})
CH_3NO_2	0.06	392 (1.8), 453 (2.6)
CH_3CN	0.08	395 (1.9), 454 (2.8)
$(CH_3)_2CO$	0.10	455 (3.1)
CH_3OH	0.18	457 (3.5)
dmf	0.19	460 (2.7)
H_2O	0.65	456 (4.7)
$(CH_3)_2CO$:H_2O mixtures		
35 mol % H_2O	0.27	456 (3.5)
52 mol % H_2O	0.32	456 (3.7)
76 mol % H_2O	0.39	456 (3.8)
91 mol % H_2O	0.54	456 (4.4)

The spectrum in dmso was not measured because of partial bleaching of the solution. That is consistent with the partial solvolysis of the complex in that solvent detected by NMR. The spectrum in ethanol was not measured because spectroscopic grade ethanol was not available.

There is a good linear relationship between the low-spin fraction and ε_{max} in the water/acetone mixtures, but data for the other pure solvents do not fit this correlation so closely.

Figure S6 below implies that compounds with $\varepsilon_{max} \approx 2.7 \times 10^3$ dm^3 mol^{-1} cm^{-1} are essentially high-spin. That is inconsistent with the NMR and Evans method data in dmf, which imply that ε_{max} in that solvent should be comparable to that in methanol. The anomalously low ε_{max} value in dmf may reflect the broadening of the MLCT peak that is clearly visible in that solvent.

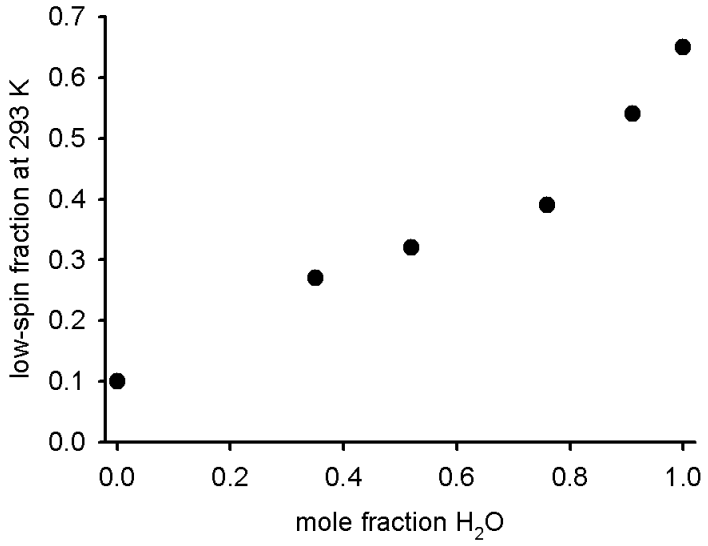

Fig. S6 Variation of the spin-state population at room temperature for $[Fe(3\text{-bpp})_2][BF_4]_2$ (**1[BF$_4$]$_2$**) with solvent composition in the water/acetone solvent mixtures. The data are taken from Table 1 in the main article.

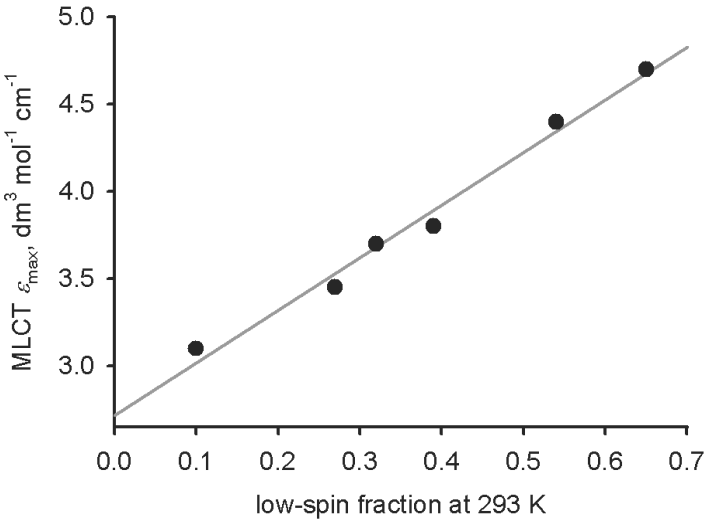

Fig. S7 Correlation between the Evans method and UV/vis data for $[Fe(3\text{-bpp})_2][BF_4]_2$ (**1[BF$_4$]$_2$**) in the water/acetone solvent mixtures.

References

[1] K. H. Sugiyarto and H. A. Goodwin, *Aust. J. Chem.*, 1988, **41**, 1645.

[2] J. M. Holland, J. A. McAllister, C. A. Kilner, M. Thornton-Pett, A. J. Bridgeman and M. A. Halcrow, *J. Chem. Soc., Dalton Trans.*, 2002, 548.

[3] G. M. Sheldrick, *Acta Crystallogr., Sect. A*, 2008, **64**, 112

[4] L. J. Barbour, *J. Supramol. Chem.*, 2001, **1**, 189.

[5] *POVRAY v. 3.5*, Persistence of Vision Raytracer Pty. Ltd., Williamstown, Victoria, Australia, 2002. http://www.povray.org.

[6] D. F. Evans, *J. Chem. Soc.*, 1959, 2003; E. M. Schubert, *J. Chem. Educ.*, 1992, **69**, 62.

[7] C. J. O'Connor, *Prog. Inorg. Chem.*, 1982, **29**, 203.

[8] J. C. Philip and H. B. Oakley, *J. Chem. Soc., Trans.*, 1924, **125**, 1189;
W. A. Felsing and S. A. Durban, *J. Am. Chem. Soc.*, 1926, **48**, 2885;
K. T. Thomas and R. A. McAllister, *AIChE J.*, 1957, **3**, 161;
T. W. Yergovich, G. W. Swift, and F. Kurata, *J. Chem. Eng. Data*, 1971, **16**, 222;
B. García and J. C. Ortega, *J. Chem. Eng. Data*, 1988, **33**, 200;
A. Marchetti, C. Preti, M. Tagllarucchi, L. Tassi and G. Tosi, *J. Chem. Eng. Data*, 1991, **36**, 360.

[9] *SIGMAPLOT*, v. 8.02, SPSS Scientific Inc., Chicago IL, 2002.

[10] C. Reichardt, *Chem. Rev.*, 1994, **94**, 2319.

[11] V. Gutmann and D. Wychera, *Inorg. Nucl. Chem. Lett.*, 1966, **2**, 257.

[12] Y. Marcus, *Chem. Soc. Rev.*, 1993, **22**, 409.

[13] J. Catalan, C. Diaz, V. López, P. Pérez, J.-L. G. de Paz and J. G. Rodriguez, *Liebigs Ann.*, 1996, 1785.

[14] M. J. Kamlet, J.-L. M. Abboud, M. H. Abraham and R. W. Taft, *J. Org. Chem.*, 1983, **48**, 2877.